Applied Catalysis B: Environmental 309 (2022) 121268

Contents lists available at ScienceDirect

Applied Catalysis B: Environmental

journal homepage: www.elsevier.com/locate/apcatb

Efficient photocatalytic epoxidation of styrene over a quantum-sized SnO_2 on carbon nitride as a heterostructured catalyst

Min Li [a,1], Lina Ma [b,1], Lan Luo [b,1], Yuguang Liu [b], Ming Xu [b], Hua Zhou [a], Ye Wang [a], Zhenhua Li [b], Xianggui Kong [b], Haohong Duan [a,*]

[a] Department of Chemistry, Tsinghua University, 30 Shuangqing Rd, Beijing 100084, China
[b] State Key Laboratory of Chemical Resource Engineering, Beijing University of Chemical Technology, Beijing 100029, China

ARTICLE INFO

Keywords:
Quantum dots
Styrene
Epoxidation
Formamide
Photocatalysis

ABSTRACT

Styrene oxide is a pivotal organic intermediate in pharmaceuticals and fine chemicals synthesis. However, the current synthesis process relies on the use of peroxy acid or chlorohydrin, which is incompatible with establishing a more sustainable chemical industry. Here, we reported the synthesis of a quantum-sized SnO_2 on 2D graphitic carbon nitride (CN) as a heterostructured catalyst, which displays efficient photocatalytic styrene epoxidation at room temperature using O_2 as a mild oxidant, achieving styrene conversion of 98.1% and styrene oxide yield of 71.8%. Photoelectrochemical analysis demonstrates efficient electron transferring exists from CN to SnO_2, which enhances charge carriers' separation and transfer processes. Furthermore, we couple the photocatalytic styrene epoxidation with epoxide ring-opening amination, achieving the synthesis of value-added β-amino alcohol in a cascade reaction fashion. This work may shed light on the heterostructured catalyst design for photocatalytic selective synthesis of valuable chemicals in a sustainable manner.

1. Introduction

Selective oxidation of organic compounds to produce value-added products is a fundamental and challenging research topic [1,2]. Styrene oxide, a main oxidative product of styrene, is an important organic intermediate which can find wide use in synthesizing perfumes, epoxy resins and plasticizer [3]. However, peroxy acid or chlorohydrin are conventionally required as the oxidants in current industrial production process, which may cause serious environmental pollution [4,5]. As a result, more sustainable catalytic methods using green oxidants like molecular oxygen (O_2) is highly desirable [6].

Over the last decade, photocatalytic methods driven by renewable solar source have aroused wide attention for H_2 production, CO_2 reduction [7,8]. Recently, photocatalytic strategy has been extended to organic synthesis to produce value-added chemicals [9–11]. In particular, photocatalytic styrene epoxidation has been shown a promising way to yield styrene oxide [12,13]. It is proposed that free radicals including $\bullet O_2^-$ and $^1O_2$ are involved in the photocatalytic reaction and contribute to the enhanced styrene epoxidation activity [5,13]. However, H_2O_2 and TBHP oxidants are used to generate the free radicals to achieve enhanced epoxidation performance [14,15]. To substitute the harsh oxidant with O_2 for epoxidation reaction, the design of photocatalyst that can effectively activate O_2 is highly important. Recently, Li and co-workers reported a perovskite structured $LaSrCo_xFe_{2-x}O_6$ material for styrene epoxidation, which shows a 100% conversion for styrene and 87.8% selectivity of styrene oxide [13]. Huang et al. reported Cu nanoparticles/TiN photocatalysts for epoxidation of styrene with 100% conversion and 53% yield of styrene oxide under visible light irradiation with air as oxidant [12]. However, these reactions were operated at elevated temperature, by which hot electrons are generated to facilitate free radicals formation from O_2. As a result, it remains challenging to design a photocatalyst that can achieve photocatalytic styrene epoxidation at room temperature by using O_2 as the mild oxidant.

Zero-dimensional (0D) semiconductor quantum dots (QDs) with unique properties of large surface area and short effective charge carrier transfer path attracts significant attention in photocatalyst designing [16,17]. It is believed that semiconductor QDs not only generate electrons and holes under light irritation, but also act as a superfast charge tunnel to enhance the separation of charge carriers [18]. However, QDs

* Corresponding author.
E-mail address: hhduan@mail.tsinghua.edu.cn (H. Duan).
[1] Min Li, Lina Ma and Lan Luo contributed equally to this work.

https://doi.org/10.1016/j.apcatb.2022.121268
Received 26 December 2021; Received in revised form 21 February 2022; Accepted 27 February 2022
Available online 2 March 2022

are often suffering from self-aggregation, instability compared with bulk materials and high photoluminescence. On the other hand, two-dimensional (2D) layered materials have gained special attentions for photocatalytic redox reactions due to the large specific surface area, which provides abundant exposed active sites and have short transfer paths for photogenerated charge carriers, thus the separation efficiency of photoinduced electrons and holes can be highly improved [19–21]. In addition, due to the existence of abundant surface defects, the adsorption of substrate on the surface of photocatalysts can be enhanced, offering higher catalytic activity. In this context, the fabrication of 0D/2D heterojunctions would not only increase the stability of QDs, but also decreases its photoluminescence inhibiting the recombination of photoexcited electrons and holes [22]. Indeed, recent progresses have demonstrated that the heterointerfaces between QDs and 2D materials provides an efficient interfacial charge transfer pathway for enhanced photocatalytic activities [23]. For example, Ma and co-workers constructed a series of 0D vanadate QDs/2D g-C_3N_4 heterojunctions which exhibits superior visible-light-driven photocatalytic degradation performance [24]. Ma and co-workers fabricated 0D CN QDs/2D g-C_3N_4 heterojunctions for efficient hydrogen peroxide evolution performance [25]. Therefore, we expect that the construction of 0D QDs/2D heterojunctions can increase the charge transfer and separation capability that promotes O_2 activation towards enhanced photocatalytic styrene epoxidation.

g-C_3N_4 has an appropriate band gap for visible light absorption, large specific surface area and ultra-thin 2D layered structure, thus is a promising photocatalyst for selective oxidation reactions [26,27]. As an n-type semiconductor, SnO_2 has a wide band gap (3.5 eV) with relatively positive valence band (VB) and conduction band (CB). The CB and VB position of SnO_2 match that of C_3N_4 to fabricate heterostructure composite, which provides a pathway of electrons from C_3N_4 to SnO_2 [28–30]. Herein, we reported a photocatalyst with 0D/2D heterojunction of SnO_2 QDs/CN composite via impregnation and calcination methods. The as-prepared SnO_2 QDs/CN shows excellent photocatalytic epoxidation activity of styrene, achieving styrene conversion (98.1%) and styrene oxide yield (71.8%) at room temperature using O_2 as the oxidant. Photoelectrochemical analysis indicates efficient electron transferring from CN to SnO_2 exists, which enhances charge carriers separation and transfer processes. Mechanistic studies show that O_2 are reduced to $\cdot O_2^-$ radical by the electrons on the CB of SnO_2, which then converts to O* as a key intermediate species for the following styrene epoxidation by the photoexcited holes. In addition, formamide (CH_3NO) is used as the solvent which plays an important role in helping to stabilize the in-situ formed O* species. Meanwhile, carbon-centered radicals are generated by activating styrene over the photoexcited holes, which combines with O* to afford styrene oxide. Based on the high efficiency of this SnO_2 QDs/CN for photocatalytic synthesis of styrene oxide, we set up a two-step reaction to synthesize a valuable molecule, β-amino alcohol, by coupling photocatalytic epoxidation of styrene with cascade epoxide ring-opening amination reaction, achieving 70.0% yield of amino alcohols under mild reaction conditions. Our work demonstrate the possibility of achieving photocatalytic styrene epoxidation under mild condition by engineering catalyst heterointerface.

2. Experimental section

2.1. Synthesis

Synthesis of C_3N_4: The C_3N_4 was synthesized by one-step thermal polymerization method via calcining urea at 520 °C for 4 h. The obtained yellow solid was grinded and denoted as CN.

Synthesis of SnO_2 QDs/CN: The SnO_2 QDs/CN samples were prepared via a wet-impregnation method. To obtain SnO_2 QDs/CN with different SnO_2 QDs loading mass, different amount of $SnCl_2$ (5 mg, 10 mg, 20 mg, 50 mg) was added into HCl solution (0.2 mL HCl in 20 mL H_2O) under stirring at room temperature. Then 0.2 g CN powder was dispersed in the above solution. After stirring for 8 h, the powders were collected, washed with deionized water and freeze-dried. Then the powder was grinded and subjected to thermal annealing in a tube furnace at 400 °C for 2 h under Ar flow. The samples with different amount of $SnCl_2$ (5 mg, 10 mg, 20 mg, 50 mg) were denoted as SnO_2 QDs/CN-X (X = 5, 10, 20, 50).

Synthesis of SnO_2 NPs (nanoparticles) /CN: 10 mg $SnCl_2$ was added in a $NaIO_3$ solution (0.2 g $NaIO_3$ and 20 mL H_2O) in the presence of 0.2 g CN under stirring at room temperature. Then the solution was stirred under the illumination of a 300 W Xe lamp for 2 h. The product was collected and washed with deionized water and dried at 60 °C. The product was denoted as SnO_2 NPs/CN.

2.2. Characterizations

The phase structure of the as-prepared samples was analyzed by X-ray diffractometer (Bruker D8 ADV ANCE) with Cu K_α radiation. The morphology and microstructure were analyzed by field-emission scanning electron microscopy (SEM, HITACHI SU-8010), transmission electron microscopy (TEM, FEI Tecnai F20), high-resolution transmission electron microscopy (HRTEM, FEI Tecnai F20) and spherical aberration correction TEM (JEM-ARM200F). UV-Vis spectrometer (Cary 5000 Varian, America) was used to obtain the UV-Vis diffuse reflectance spectra (DRS) of samples. The fourier-transform infrared (FTIR) spectra were recorded by a spectrometer in the range of 600–4000 cm^{-1}. The loading mass of Sn were measured by inductively coupled plasma-atomic emission spectrometer (ICP-AES) on ELAN DRC-e. The X-ray photoelectron spectroscopy (XPS) measurements were performed on a Termo escalab 250Xi. The surface photovoltage spectroscopy (SPV) was conducted through AFM (Bruker Dimension Icon, GER) analysis with the photo-assisted (300 W Xe lamp) Kelvin probe force microscopy (KPFM). The photoluminescence emission spectra and fluorescence decay spectra were investigated and measured by a fluorescene spectrophotometer and fluorescence decay spectrometer (FLS1000/FS5).

2.3. Photoelectrochemical measurements

The photocurrent and electrochemical impedance spectra were collected by electrochemical workstation (CHI660) using a three-electrode system. Specifically, an Ag/AgCl electrode and a platinum plate (1 cm* 1 cm) were used as a reference electrode and counter electrode, respectively. The series of samples films were coated on indium-tin oxide (ITO) sheet glasses using as the working electrodes. The electrolyte solution was 0.5 M Na_2SO_4. 4 mg of catalyst was added to 0.6 mL nafion ethanol solution with ultrasonication for 30 min. Then the catalyst was dripped onto the ITO glass and dried in air. After that, the ITO glass was dried in the oven at 80 °C for 2 h. A 300 W Xe lamp with AM 1.5G filter was used for testing.

2.4. Photocatalytic epoxidation of styrene

Photocatalytic epoxidation of styrene experiments was carried out in a photocatalytic reaction equipment (PCX50C Discover, Perfectlight Technology Co.) under 455 nm LED light with a total power of 6 W. Typically, 5 mg catalyst was dispersed in 2 mL formamide in a 10 mL sealed quartz reactor. Then, the reactor was vacuumed and then filled with pure O_2. After that, 0.1 mmol styrene was injected into the reactor using a micro-syringe. Then the reactor was posited in the photocatalytic reaction with stirring under light illumination. A circulating constant water system was used to keep the reactor system at 25 °C. After the reaction is completed, 1 mL 0.01 mmol/mL mesitylene in formamide solvent was added into the liquid mixture as an analytical internal standard. The liquid was then filtered and analyzed by gas chromatography-mass spectrometry (GC-MS, Agilent Technologies, GC7890B, MS 5977B) with HP-5 column (30 m*0.25 mm*0.25 μm) and FID detector. The styrene epoxidation experiment under solar light was

conducted in a ten-fold scale.

2.5. Stability experiment

For the stability experiments using SnO_2 QDs/CN as the catalyst, after each reaction cycle, the spent catalyst was separated by centrifugation, dried in a vacuum oven at 60 °C for 10 h and then used for the next cycle. The liquid products were collected and analyzed by GC-MS.

2.6. Synthesis experiment of β-amino alcohol (1-phenyl-2-(phenylamino) ethanol)

Firstly, photocatalytic styrene epoxidation was performed in a quartz reactor under the same conditions as shown above. When the reaction was completed, 1 mmol aniline and 20 mg $CeCl_3$ were added into the reactor. The reactor was vacuumed and then the reaction was conducted under darkness for 8 h. After the reaction, the liquid mixture was filtered by a 0.22 μm filter, and 7 μL mesitylene was added in the solution. Then 50 μL of the solution was extracted and mixed with 0.7 mL $CDCl_3$, and analyzed by 600 M NMR spectrometers (JNM-ECA600).

3. Results and discussion

3.1. Synthesis and characterization

The synthesis procedure of SnO_2 QDs/CN follows a wet-impregnation and calcination method (Fig. 1a). We speculate the formation of SnO_2 in Ar atmosphere derives from the decomposition of the hydrolysis product of $SnCl_2$ during the synthesis. To verify this assumption, we prepared high amounts of $SnCl_2$ in water and observed an obvious hydrolysis reaction. XRD shows that the hydrolysis product of $SnCl_2$ displays a phase of $Sn_{21}Cl_{16}(OH)_{14}O_6$ (Fig. S1). The hydrolysis product was not obvious in the calcination precursor of SnO_2 QDs/CN, which might be attributed to the low Sn loading mass and small particle size. The SnO_2 QDs/CN-10 was used for further structure characterization for its higher activity (as shown below). SnO_2 NPs/CN were prepared by a photo-deposition method. The synthesis details are shown in the experimental section. The loading mass of Sn in SnO_2 QDs/CN-10 and SnO_2 NPs/CN samples were determined to be 1.78 wt% and 0.91 wt%, respectively, measured by ICP-AES (Fig. S2). XRD patterns of CN, SnO_2 QDs/CN-10 and SnO_2 NPs/ CN photocatalysts show two obvious peaks at around 13° and 27.5°, which are well indexed to the (100) and (002) of CN (Fig. S3) [31]. The peak of SnO_2 is not detectable, an indicative of ultra-small size of Sn species. The optical property of CN, SnO_2 QDs/CN-10 and SnO_2 NPs/ CN was evaluated by DRS (Fig. S4). Compared to the photoabsorption of SnO_2 NPs/CN, the photoabsorption of SnO_2 QDs/CN-10 displays a slight blue shift, which is due to the quantum confinement effect [24]. The morphology of SnO_2 QDs/ CN-10 shows typical CN lamellar structure by SEM (Fig. S5). HRTEM image shows the quantum dots on the surface of CN (Fig. 1b). Elemental mapping images of SnO_2 QDs/CN-10 confirms the uniform distribution of Sn on CN (Fig. 1c). To observe the quantum-sized SnO_2, spherical aberration correction TEM was conducted (Fig. 1d). The images clearly show that SnO_2 with quantum dot-sized QDs are supported on CN. It reveals that the lattice spacing of SnO_2 QDs is about 0.330 nm, corresponding to the (110) planes of SnO_2 (Fig. 1d). The statistical particle size distribution of SnO_2 were counted based on about 140 dots with an average diameter of 2.2 nm, revealing a typical quantum size (Fig. 1d inset and Fig. S6). The quantum size of SnO_2 would be beneficial for the formation of abundant heterointerfaces between the SnO_2 and CN. As a reference catalyst, SnO_2 NPs/CN was synthesized by photo-deposition method (Fig. S7a, b). Elemental mapping images further confirm the elemental composition and distribution of SnO_2 NPs/CN (Fig. S7c). The average diameter and standard deviation of SnO_2 NPs are 42.3 nm and 9.0 nm, respectively (Fig. S7d).

The strong interaction between SnO_2 QDs and CN in SnO_2 QDs/CN-10 is reflected by XPS (Fig. S8). Two peaks at the binding energies of 284.8 and 288.2 eV in C 1 s high resolution spectra are fitted to the C−C bond from the adventitious carbon and hybridized carbon in the aromatic ring (N − C═N), respectively (Fig. 2a) [32]. In N 1 s high-resolution spectra, three typical peaks at 398.57 eV, 399.43 eV and 401.12 eV are attributed to C−N═C, N − $(C)_3$ and C−NH_2, respectively (Fig. 2b). In Sn 3d XPS spectra, the binding energies at 495.86 eV and 486.75 eV are attributed to Sn^{4+} 3d 3/2 and 3d 5/2 (Fig. 2c) [33].

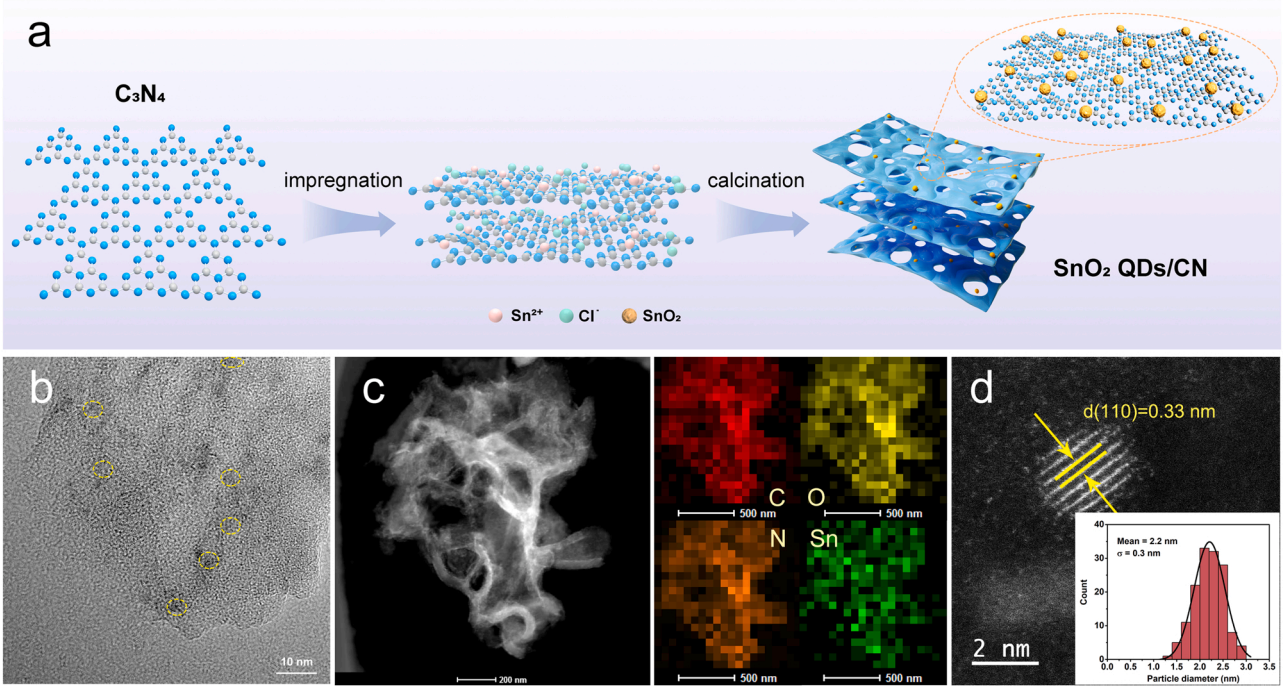

Fig. 1. a) Schematic illustration of synthesis SnO_2 QDs/CN; b) TEM image, c) TEM image and elemental mapping, d) STEM image of SnO_2 QDs/CN-10 (inset: Size distribution).

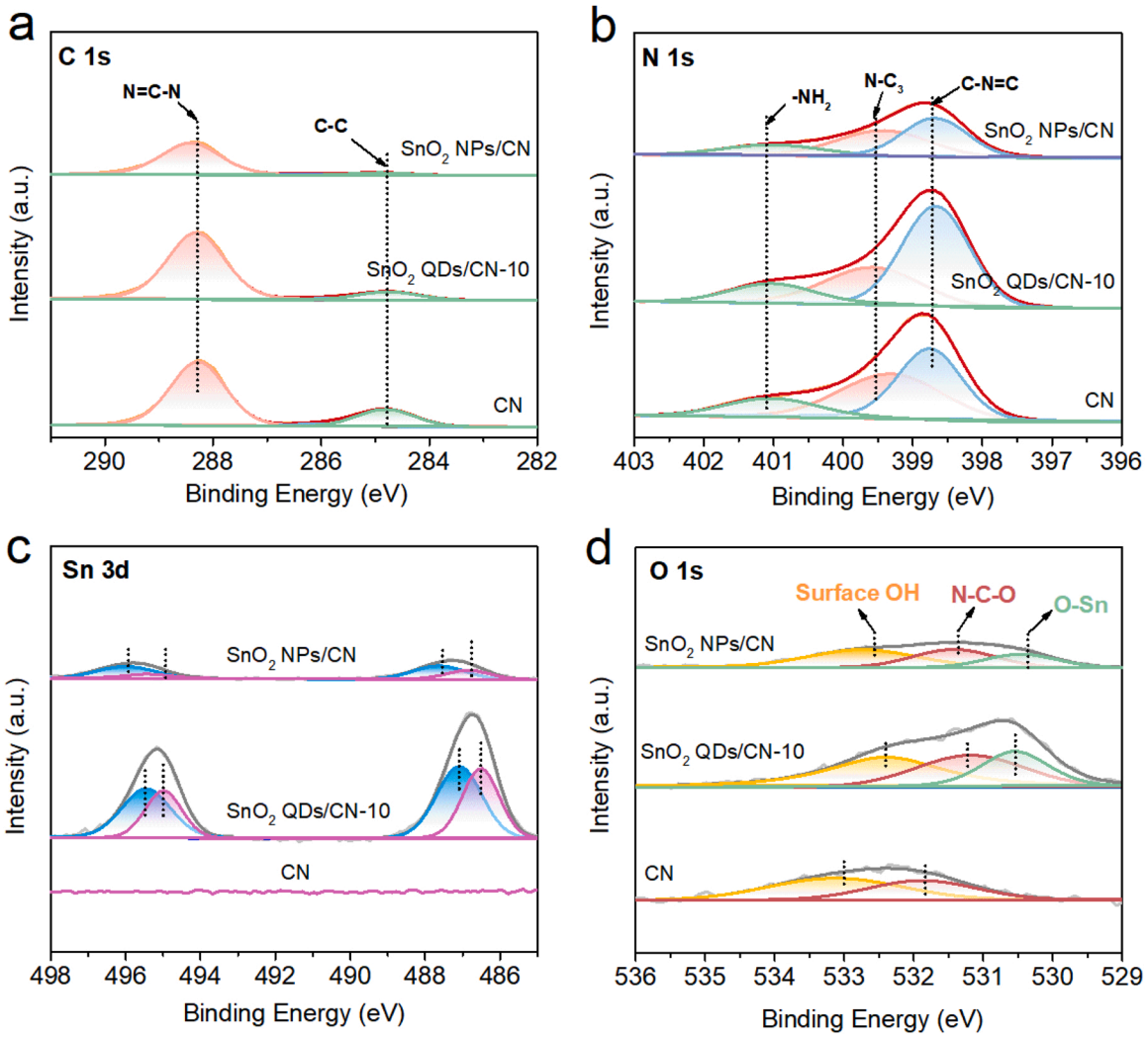

Fig. 2. XPS spectra of a) C 1s; b) N 1s; c) Sn 3d; d) O 1s.

Obviously, other two peaks demonstrate the generation of a lower binding energy of Sn^{4+}, which is due to the formation of Sn−N bond in SnO_2 QDs/CN-10. The intensity of Sn 3d peaks in SnO_2 QDs/CN-10 is higher than that in SnO_2 NPs/CN, indicating higher content of Sn in SnO_2 QDs/CN-10. The evident negative shifts of binding energy of Sn peaks in SnO_2 QDs/CN-10 than in SnO_2 NPs/CN suggest a higher

Table 1
Photocatalytic styrene epoxidation performance of different semiconductors.

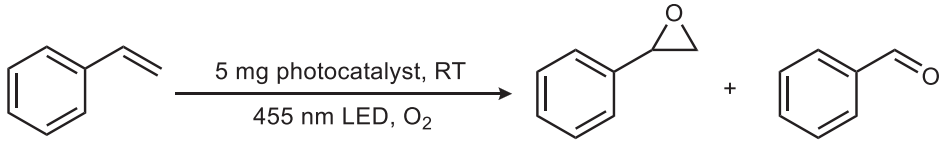

1a 2a 3a

Entry	Catalyst	Solvent	Conv. (%)	**2a** Yield (%)	**3a** Yield (%)
1	BiOCl	CH_3NO	34.7	26.6	8.1
2	TiO_2	CH_3NO	50.6	45.7	4.9
3	$W_{18}O_{49}$	CH_3NO	41.7	36.8	4.9
4	$BiVO_4$	CH_3NO	56.0	45.7	10.3
5	$ZnIn_2S_4$	CH_3NO	59.2	35.3	23.9
6	MoS_2	CH_3NO	55.0	39.3	15.7
7	CdS	CH_3NO	58.8	32.2	26.6
8	CN_m	CH_3NO	49.0	32.6	16.4
9	CN_t	CH_3NO	30.5	19.0	11.5
10	CN	CH_3NO	61.9	45.8	16.1

Reaction conditions: 5 mg of catalysts, 0.1 mmol of styrene, 2 mL solvent, 455 nm LED, O_2, 12 h (CN_m, CN_t and CN represent C_3N_4 derived from melamine, thiourea and urea, respectively).

electron density over Sn in SnO_2 QDs/CN-10 [34]. O 1s spectra are fitted to three peaks, which can be assigned to surface OH, N − C−O in CN introduced by the process of urea calcination and O−Sn bond, respectively (Fig. 2d). These results clearly show the close contact between SnO_2 and CN through the formation of heterointerfaces, which may facilitate electron transfer from CN to SnO_2, thus enabling SnO_2 to serve as a good electron acceptor for O_2 reduction in styrene epoxidation.

3.2. Evaluation of photocatalytic performance

The conversion of styrene into styrene oxide is of paramount significance in the chemical industry. In this reaction, styrene oxide (**2a**) is the desired product and benzaldehyde (**3a**) is the by-product. Several typical semiconductors (TiO_2, CdS, $BiVO_4$, BiOCl, $W_{18}O_{49}$, MoS_2, C_3N_4) were firstly synthesized and screened for photocatalytic epoxidation of styrene under 455 nm LED irradiation at room temperature (Table 1, entry 1–10), by using O_2 as oxidant and formamide as the solvent. The catalytic results show that CN derived from urea calcination exhibits the highest conversion rate of 61.9% and styrene oxide yield of 45.8% compared to other semiconductors.

The solvent was also optimized by using N, N-dimethylformamide (DMF), dimethyl sulfoxide (DMSO), acetonitrile (CH_3CN), 1,4-dioxane and CH_3NO (Table 2, entry 1–5). CN_3NO shows higher **1a** conversion and **2a** yield, which can be probably attributed to the high polarity of CH_3NO with good oxygen solubility [35]. Using CH_3NO as the solvent, compared with CN and SnO_2 NPs/CN, SnO_2 QDs/CN-10 shows higher **1a** conversion (67.5%) and yield of **2a** (53%) for 8 h reaction (Table 2, entry 6–8), suggesting that introducing QDs can obviously improve the activity of photocatalytic epoxidation. In contrast, SnO_2 NPs exhibits no styrene epoxidation activity at the same conditions, indicating that SnO_2 alone can't be excited by visible light (Table 2, entry 9). To reveal the effect of particle size and distribution on catalytic performance, the epoxidation activities of quantum-sized SnO_2 (2.2 nm) and nanoparticles (42.3 nm) were compared, as well as an additional quantum-sized SnO_2 (4.0 nm, shown in Fig. S9). The catalytic results of three catalysts are provided in Table S1 as entry 2, 4 and 3, respectively, showing that SnO_2 with smaller size exhibits better epoxidation performance, probably due to the shorter charge carrier transfer path and quantum size effect. In addition, the reaction time was prolonged for gaining higher conversion (Table 2, entry 10–12 and Table S1 1–3 and 5–7). Notably, the results show that **1a** conversion of 98.1% and **2a** yield of 71.8% were achieved after 24 h over SnO_2 QDs/CN-10, which represents a superior photocatalytic performance compared with mostly reported catalysts in epoxidation of styrene (Table S2). We synthesized a SnO_2 NPs/CN sample with high loading SnO_2 NPs with the Sn content of 38.3 wt%, which is much higher than that the Sn content in SnO_2 QDs/CN-10. However, this sample affords styrene conversion of 58.4% and styrene oxide yield of 34.0% (Table S1, entry 8), which are both lower than that of SnO_2 QDs/CN-10 (78.2% of styrene conversion and 58.4% of styrene oxide yield, as shown in Table S1, entry 2). In addition, the effect of Sn loading mass in SnO_2 QDs/CN on catalytic activity was also examined, by the comparison of SnO_2 QDs/CN-5, SnO_2 QDs/CN-10, SnO_2 QDs/CN-20 and SnO_2 QDs/CN-50 with different Sn loading but similar particle size (Table 2 entry 13–15). The catalytic results show that SnO_2 QDs/CN-10 exhibits the highest activity. These results further indicate that the loading mass of Sn has insignificant effect on the catalytic performance, and SnO_2 QDs with even higher loading amount would result in aggregation that blocks the active sites of CN as shown by TEM (Fig. S10), which in turn decrease catalytic activity for epoxidation reaction. We also investigated the influence of calcination temperature during SnO_2 QDs/CN preparation on the activity, by comparing the SnO_2 QDs/CN-10 calcined at 200, 300, 400 and 500 °C for epoxidation (Table S1 entry 9–12). The results display that SnO_2 QDs/CN-10 calcined at 400 °C has the best epoxidation performance. In addition, we studied the source of oxygen for epoxidation, by conducting the reaction at different atmospheres (Table 2, entry 16). No styrene epoxidation activity was observed under Ar atmosphere, indicating that the oxygen atom in the styrene oxide is derived from O_2 molecular. When the reaction system was heated at 60 °C, a dramatically increased **1a** conversion (83.7%) and **2a** yield (70.0%) was observed (Table 2, entry 17). This result reflects that the activity can be promoted by hot electrons via thermal strategy. Furthermore, ten-fold reaction was conducted under solar light irradiation (Table 2, entry 18). The **1a** conversion could reach 52.0% with the **2a** yield of 47.3%, suggesting the potential of the catalyst under practical photocatalytic condition for efficient styrene epoxidation.

Table 2
Optimization of styrene epoxidation reaction conditions.

Entry	Catalyst	Solvent	Time	Conv. (%)	**2a** Yield (%)	**3a** Yield (%)
1	CN	DMF	16 h	26.3	8.6	17.7
2	CN	CH_3NO	16 h	70.1	52.6	17.5
3	CN	DMSO	16 h	84.5	13.9	70.6
4	CN	1,4-dioxane	16 h	24.9	4.3	20.6
5	CN	CH_3CN	16 h	43.9	14.6	29.3
6	CN	CH_3NO	8 h	42.8	30.3	12.5
7	SnO_2 QDs/CN-10	CH_3NO	8 h	67.5	53.0	14.5
8	SnO_2 NPs/CN	CH_3NO	8 h	46.4	31.8	14.6
9	SnO_2	CH_3NO	8 h	0	0	0
10	CN	CH_3NO	24 h	87.8	66.0	21.8
11	SnO_2 QDs/CN-10	CH_3NO	24 h	98.1	71.8	26.3
12	SnO_2 NPs/CN	CH_3NO	24 h	81.7	61.4	20.3
13	SnO_2 QDs/CN-5	CH_3NO	8 h	62.1	47.4	14.7
14	SnO_2 QDs/CN-20	CH_3NO	8 h	65.2	48.0	17.2
15	SnO_2 QDs/CN-50	CH_3NO	8 h	67.1	46.5	20.6
16[a]	SnO_2 QDs/CN-10	CH_3NO	8 h	0	0	0
17[b]	SnO_2 QDs/CN-10	CH_3NO	8 h	83.7	70.0	13.7
18[c]	SnO_2 QDs/CN-10	CH_3NO	8 h	52.0	47.3	4.7

Standard Reaction conditions: 5 mg of catalysts, 0.1 mmol of styrene, 2 mL solvent, 455 nm LED, O_2.
[a] Reaction at Ar atmosphere.
[b] Reaction at 60 °C.
[c] Reaction under sunlight, 50 mg SnO_2 QDs/CN-10, 1 mmol of styrene, 20 mL CH_3NO, O_2.

3.3. Photocatalytic epoxidation of different substrates

To demonstrate the general applicability of the SnO_2 QDs/CN-10, a series of alkene substrates were tested under the optimized reaction conditions at different reaction times (Table 3). Generally, cycloalkenes are more active in epoxidation reactions, which is due to their high electron densities have a positive effect on the electrophilic oxygen transfer, leading to enhanced reactivity. High conversions were obtained for cyclohexene and cycloheptene with the 100% selectivity of epoxidation products (Table 3, entries 1 and 2). Increasing the strain energy of cycloalkanes can improve the reaction efficiency, such as norbornene, which exhibits good epoxidation activity (Table 3, entry 3). Long chain alkenes also show promising epoxidation performances (Table 3, entries 4 and 5). However, the terminal alkenes display lower epoxidation activity than cycloalkenes, which is due to the low electron densities (Table 3, entries 6–8). The yield of epoxy product is slightly lower, which is due to some products are not detectable. Notably, SnO_2 QDs/CN-10 shows promising epoxidation of nonterminal inner alkenes such as stilbenes, which usually have steric hindrance issue (Table 3,

Table 3
Scope of epoxidation reactions of alkenes.

[1] 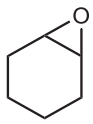 Conv. 83.4 % Sel. 100 %	[2] 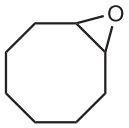 Conv. 88.5 % Sel.100 %	[3] 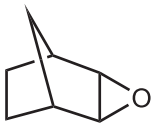 Conv. 93.6 % Sel.100 %	[4] 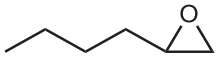 Conv. 89.1 % Sel.100 %
[5] 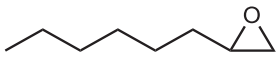 Conv. 93.7 % Sel.100 %	[6] 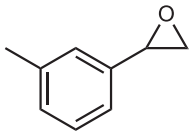 Conv. 86.0 % Sel.80.4 %	[7] 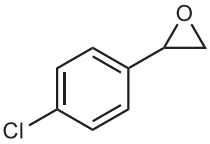 Conv. 40.0 % Sel.77.8 %	[8] 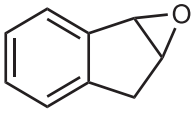 Conv.99 % Sel.78.3 %
[9] 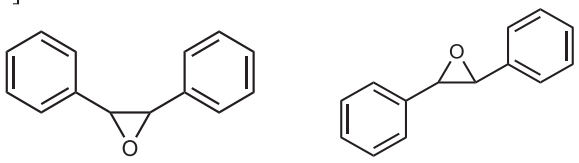 *trans*- Conv. 100 % *cis*- Sel. 10.9 %, *trans*- Sel. 33.5 % *cis:trans*=0.3:1		[10] 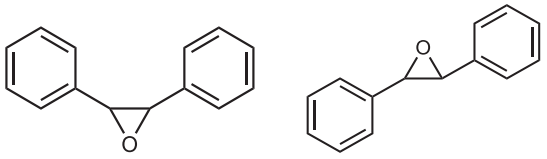 *cis*- Conv. 51.8 % *cis*- Sel. 59.3 %, *trans*- Sel. 19.1 % *cis:trans*=3.1:1	

Reaction Conditions: 5 mg SnO_2 QDs/CN-10, 0.1 mmol of substrate and 2 mL CH_3NO, 455 nm LED, O_2 [1–3]. reaction for 24 h [6–10]. reaction for 16 h [4,5]. reaction for 8 h. Conversion and selectivity of [1–5] and [9,10] were determined by GCMS analysis. Conversion and selectivity of [6–8] were determined by ^{1}H NMR.

entries 9 and 10). *Cis*-stilbenes and *trans*-stilbenes could convert to corresponding isomerization under light irradiation. We observed only 10.9% selectivity of *cis*-epoxidation products in the *trans*-stilbenes epoxidation reactions and 19.1% selectivity of *trans*-epoxidation products in the *cis*-stilbenes epoxidation reactions, suggesting that the conversion from *trans* to *cis* is more difficult due to the higher energy barrier [12].

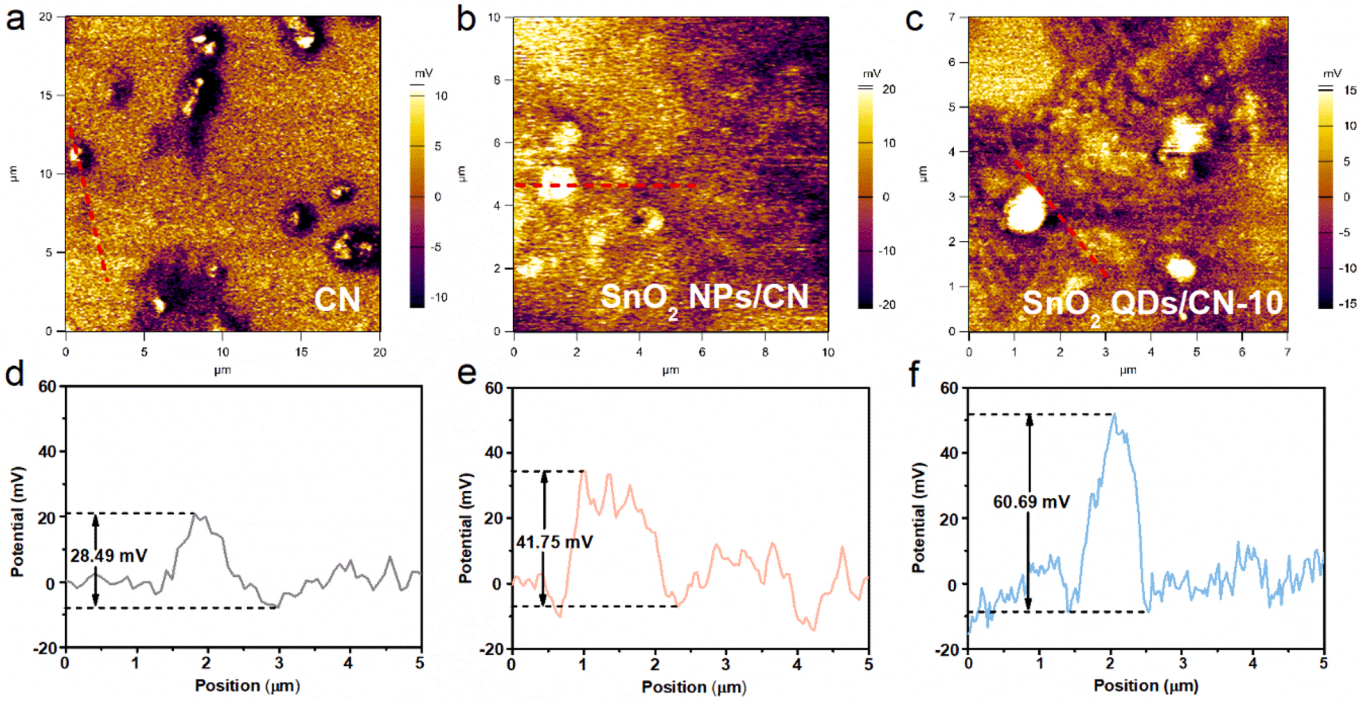

Fig. 3. The SPV images and corresponding potential difference of a, d) CN, b, e) SnO_2 NPs/CN and c, f) SnO_2 QDs/CN-10 under light irradiation.

3.4. Investigation on charge separation behaviors

To investigate the separation and transfer of charge carriers, SnO_2 QDs/CN-10 was analyzed by a series of photoelectrochemical tests. Surface photovoltage spectroscopy was employed to evaluate the separation and transfer behavior of the photoinduced charge carriers [36]. CN, SnO_2 QDs/CN-10 and SnO_2 NPs/CN show the SPV response under light illumination (Fig. 3a~f, Fig. S11). SnO_2 QDs/CN-10 shows a larger potential difference of 60.7 mV compared with CN (28.5 mV) and SnO_2 NPs/CN (41.75 mV), suggesting that SnO_2 QDs help to restrain the recombination of bulk electron-hole pairs, facilitating the transfer of electrons from CN to SnO_2. It is believed that the accumulation of electrons on SnO_2 and holes on CN promotes the styrene adsorption and oxidation on the photocatalysts [37]. The transient photocurrent response of SnO_2 QDs/CN-10 is greatly strengthened in comparison with that of CN and SnO_2 NPs/CN, demonstrating that the photogenerated charge carriers of SnO_2 QDs/CN-10 are efficiently separated by supporting SnO_2 QDs on CN (Fig. 4a) [38,39]. In electrochemical impedance spectroscopy (EIS), compared with CN and SnO_2 NPs/CN, the SnO_2 QDs/CN-10 exhibits smaller radius, indicating a higher interfacial charge transfer efficiency (Fig. 4b) [40]. PL spectra of the samples show that the emission intensities are reduced after supporting SnO_2 on CN, reflecting a dramatically lowered charge recombination rate [41]. The fast charge recombination, which is considered a historical intrinsic drawback of CN, can be largely overcome by combining with SnO_2 QDs (Fig. 4c). The charge separation dynamics of CN, SnO_2 QDs/CN-10 and SnO_2 NPs/CN were also investigated by the time-resolved fluorescence decay spectra (Fig. 4d). The τ_1 and τ_2 represent the life time of bulk separation carriers in CN and life time of carriers transfer from CN to SnO_2. Compared with CN and SnO_2 NPs/CN, SnO_2 QDs/CN-10 has a relatively short τ_1 life time (2.10 ns) and longest τ_2 life time (10.60 ns), suggesting that more efficient electron transfer between CN and SnO_2 QDs. As a consequence, SnO_2 QDs/CN-10 exhibits the longest average charge carriers' life time (2.48 ns) among CN, SnO_2 QDs/CN-10 and SnO_2 NPs/CN. These photoelectrochemical results confirm that the combination of SnO_2 QDs with CN greatly facilitates separation and migration of charge carriers, which are crucial to the enhanced of photocatalytic styrene epoxidation activity [42,43]. Moreover, the stability of SnO_2 QDs/CN-10 were also tested for five cycles. As shown in Fig. 4a, the **1a** conversion and the yield of **2a** were largely maintained, demonstrating the good stability of the SnO_2 QDs/CN-10 (Fig. 5a).

3.5. Stability and photocatalytic mechanism

It is believed that radical species take a dominant role in the process of photocatalytic styrene epoxidation. However, much attentions have been focused on oxygen active species in previous works, and less on free radicals at the styrene terminal. As a result, the formation of styrene oxide is usually considered as the combination of styrene and oxygen active species directly. To comprehensively investigate the reaction mechanism, a series of control experiments was carried out (Fig. 5b). When the 2, 2, 6, 6-tetramethyl-1-piperidinyloxy (TEMPO) was added in the standard reaction as a radical scavengers, the reaction was greatly inhibited, indicating that the reaction following a radical-catalyzed pathway [44]. To differentiate the active species in epoxidation reaction, $(NH_4)_2C_2O_4$, $K_2S_2O_8$, tert-butanol (TBA), benzoquinone (BQ) and butylated hydroxytoluene (BHT) were added as scavengers to trap h^+, e^-, $\cdot OH$, $\cdot O_2^-$ and carbon-centered radical, respectively [45]. The conversion of styrene were suppressed after the scavengers of $(NH_4)_2C_2O_4$, BQ and BHT were added, indicating that h^+, $\cdot O_2^-$ and carbon-centered radical play important roles in the process of epoxidation reaction [46]. The EPR with DMPO (5, 5-dimethyl-1-pyrroline N-oxide) as spin-trapping

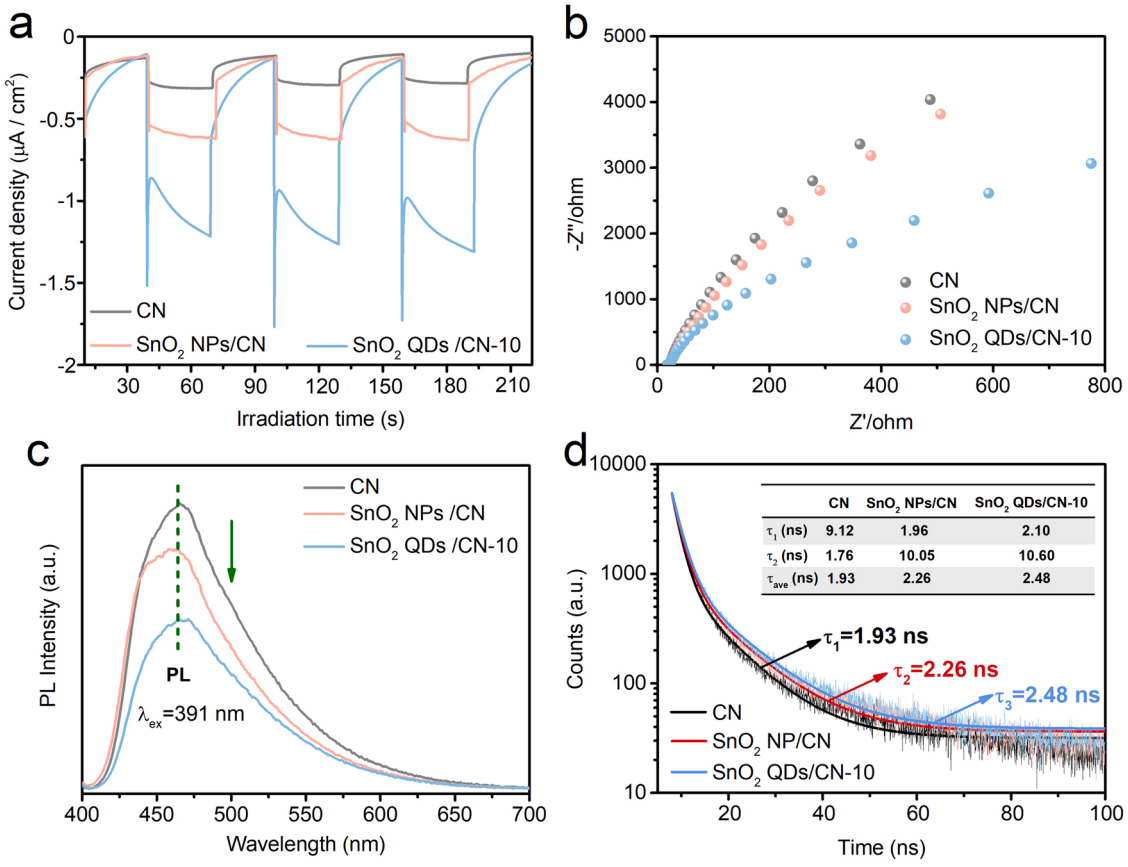

Fig. 4. a) Photocurrent density, b) EIS Nyquist plots, c) PL spectra excited at 391 nm and d) Time-resolved photoluminescence decay spectra of CN, SnO_2 QDs/CN-10 and SnO_2 NPs/CN.

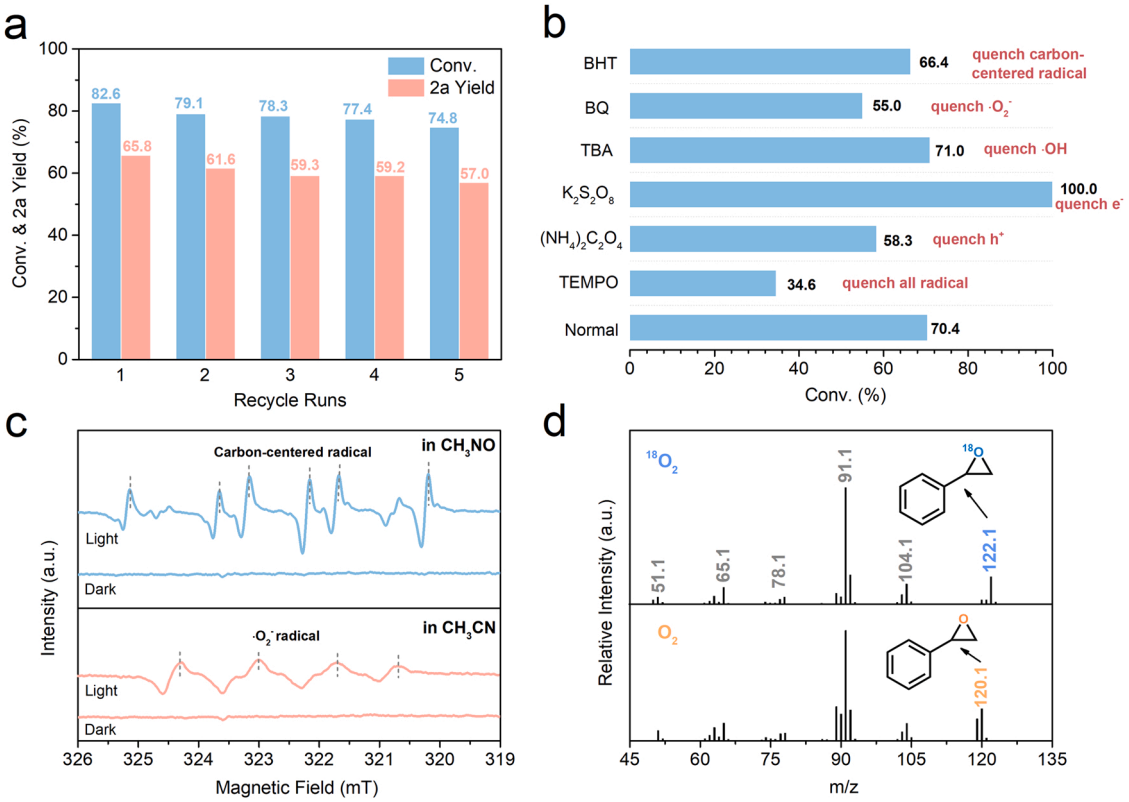

Fig. 5. a) Recycle runs of SnO_2 QDs/CN-10 during styrene epoxidation; b) The conversion of styrene oxidation with the addition of the scavengers contrast to the general condition; c) EPR detection of carbon-centered radical in CN_3NO solvent and·O_2^- radical in CH_3CN solvent using DMPO as spin-trapping agent; d) Mass spectra of styrene oxide of SnO_2 QDs/CN-10 with using $^{18}O_2$ and O_2 as reacting gas.

agent was conducted, further consolidating the active species trapping experiment results (Fig. 5c) [47]. Strong carbon-centered radical signal was observed in CH_3NO solvent under light irradiation. The signal of·O_2^- may coincide with that of carbon-centered radicals or too weak to be distinguished. Based on the results of active species trapping experiments, it is proposed that photogenerated holes play important roles in activation styrene molecule into carbon-centered radical and in reacting with·O_2^- to generate O* (which is stabilized in the CH_3NO solvent) [48]. So the·O_2^- species were not observed by EPR. In contrast, strong·O_2^- radical signal was observed when using CH_3CN as the solvent under light irradiation [49]. Considering the low selectivity of styrene oxide and high selectivity of benzaldehyde in CH_3CN, it can be concluded that·O_2^- radical plays a key role in generating benzaldehyde. Furthermore, when styrene oxide was used as the substrate, benzaldehyde was not obtained under LED irradiation (Fig. S12). These results suggest that the reaction pathways to generate benzaldehyde and styrene oxide are independent, rather than first converting to styrene oxide and then to benzaldehyde. Thus, O* and·O_2^- radical are assigned as active species in the formation of styrene oxide and benzaldehyde, respectively. Recently, it was reported that 1, 4-dioxane solvent converted to 1, 4-dioxane-peroxide with O_2, which then released oxygen adatoms (O_a) which acts as the oxidant in styrene epoxidation [12]. However, we didn't observe the formamide-peroxide by GC-MS, indicating that CH_3NO plays the role of stabilizing O* as the active species rather than reacting with O_2. To confirm the oxygen source in the photocatalytic product, the epoxidation experiment was carried out under $^{18}O_2$ atmosphere. As shown in Fig. 5d, the peak of 122.1 mass-to-charge ratio (m/z) was observed, which is assigned to styrene oxide with ^{18}O. Meanwhile, the peak of $m/z = 108$ was also observed, which is assigned to benzaldehyde with ^{18}O (Fig. S13), indicating the oxygen atom in benzaldehyde also comes from O_2. In addition, no products were detected when the catalytic reaction was performed under Ar condition, implying that the oxygen in styrene oxide and benzaldehyde derives from the O_2 molecules rather than CH_3NO.

The relative band positions of C_3N_4 and SnO_2 in Fig. 6 were obtained based on the analysis results of band gap energies (Fig. S14a, b), the VB-XPS measurement (Fig. S14c) and Mott-Schottky method (Fig. S14d). Based on the above mechanistic studies and previous literatures, the reaction mechanism of styrene oxide in CH_3NO is proposed (Fig. 6). Firstly, styrene adsorbed on the surface of CN, which is followed by styrene activation by photogenerated holes of CN to form carbon-centered radical. In the presence of SnO_2 QDs, the photogenerated electrons excited in CN can be easily transferred to SnO_2 QDs via abundant heterointerfaces, facilitating the activation of O_2 to ·O_2^- radicals. The photogenerated holes retained on the CN activate styrene and react with ·O_2^- to form O* radicals. Then the carbon-centered radicals combined with O* to yield styrene oxide. As for the reaction pathway to produce benzaldehyde as the byproduct, the carbon-centered radical cation combined with the ·O_2^- in a [2 + 2] cycloaddition manner, which gives benzaldehyde by cleavage of dioxetane (Fig. S15) [50].

3.6. Synthesis of β-amino alcohol (1-phenyl-2-(phenylamino)ethanol)

The three-membered ring of epoxide could be activated by nucleophilic attack to synthesize 1, 2-disubstituted compounds due to the high strain [51]. It is considered that β-Amino alcohols are important intermediates in pharmaceuticals, amino acids and chiral auxiliaries. To synthesize the β-amino alcohols, nucleophilic opening of epoxides with amines is a well-recognized strategy [52]. Based on the above promising catalytic results in photocatalytic styrene epoxidation over SnO_2 QDs/CN-10, we design a cascade reaction to synthesize β-amino alcohol, by combining photocatalytic epoxidation of styrene at optimized conditions with cascade epoxide ring-opening amination by using $CeCl_3$ as the catalyst under vacuum condition (Fig. 7). The conversion of styrene

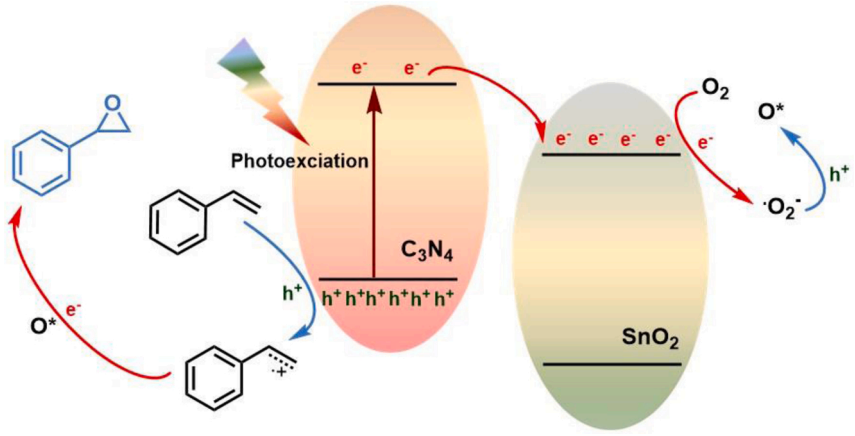

Fig. 6. Schematic diagram of reaction process of photocatalytic epoxidation of styrene to styrene oxide.

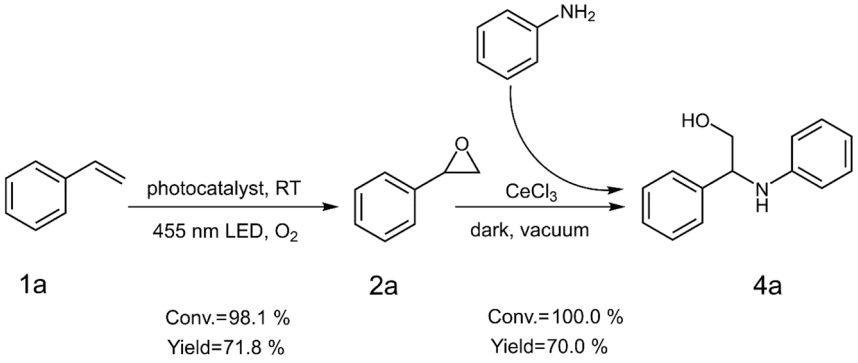

Fig. 7. Photocatalytic epoxidation of styrene and coupling reactions with target product of amino alcohol.

oxide and yield of β-amino alcohol reach 100.0% and 70.0%, respectively. This cascade strategy may provide a promising pathway for high-valued organics synthesis.

4. Conclusions

In summary, we synthesized a quantum-sized SnO_2 on 2D CN composite photocatalyst, which shows excellent styrene epoxidation performance under room temperature with O_2 as oxidant. In addition, SnO_2 QDs/CN shows substrate universality for cycloalkanes, norbornene and long chain alkenes. The construction of SnO_2 QDs/CN heterojunction enables the electron flow from CN to SnO_2, leading to high charge separation and transfer efficiencies in SnO_2 QDs/CN. The effective separation of charge carrier facilities the separation thermodynamics of charge carriers and endows more electrons and holes participated in the generation of free radicals. We attempted to couple photocatalytic styrene epoxidation with ring-opening amination reaction to produce amino alcohol using a cascade strategy, showing promising catalytic results. This work provides novelty for photocatalyst design via constructing 0D QD/2D structure with abundant heterointerface, with improved catalytic performance in photocatalytic synthesis of value-added organic chemicals.

CRediT authorship contribution statement

Min Li: Conceptualization, Investigation, Formal analysis, Writing – original draft . **Lina Ma:** Formal analysis, Data curation. **Lan Luo:** Validation, Data curation. **Yuguang Liu:** Investigation. **Ming Xu:** Formal analysis. **Hua Zhou:** Validation. **Ye Wang:** Validation. **Zhenhua Li:** Validation. **Xianggui Kong:** Validation. **Haohong Duan:** Supervision, Writing – review & editing, Project administration.

Declaration of Competing Interest

The authors declare that they have no known competing financial interests or personal relationships that could have appeared to influence the work reported in this paper.

Acknowledgements

This work was supported by the National Natural Science Foundation of China, China (Grant Nos. 53337000121, 21978147, 21935001, 22108008 and 22090031) and China Postdoctoral Science Foundation, China (043260440).

Appendix A. Supporting information

Supplementary data associated with this article can be found in the online version at doi:10.1016/j.apcatb.2022.121268.

References

[1] Z. Tian, C. Han, Y. Zhao, W. Dai, X. Lian, Y. Wang, Y. Zheng, Y. Shi, X. Pan, Z. Huang, H. Li, W. Chen, Efficient photocatalytic hydrogen peroxide generation coupled with selective benzylamine oxidation over defective ZrS_3 nanobelts, Nat. Commun. 12 (2021) 2039, https://doi.org/10.1038/s41467-021-22394-8.
[2] T. Song, C. Wang, Y. Zhang, X. Shi, Y. Li, Y. Yang, Visible-light-induced oxidative alkene difunctionalization to access α-sulfonyloxy ketones catalyzed by oxygen-vacancy-rich Nb_2O_5, Appl. Catal. B: Environ. 304 (2022), 120964, https://doi.org/10.1016/j.apcatb.2021.120964.
[3] W.R. Leow, Y. Lum, A. Ozden, Y.H. Wang, D.H. Nam, B. Chen, J. Wicks, T. T. Zhuang, F.W. Li, D. Sinton, E.H. Sargent, Chloride-mediated selective electrosynthesis of ethylene and propylene oxides at high current density, Science 368 (2020) 1228–1233, https://doi.org/10.1126/science.aaz8459.
[4] M.D. Hughes, Y.J. Xu, P. Jenkins, P. McMorn, P. Landon, D.I. Enache, A.F. Carley, G.A. Attard, G.J. Hutchings, F. King, E.H. Stitt, P. Johnston, K. Griffin, C.J. Kiely,

Tunable gold catalysts for selective hydrocarbon oxidation under mild conditions, Nature 437 (2005) 1132–1135, https://doi.org/10.1038/nature04190.
[5] Q. Wang, X. Deng, W. Chen, P. Chen, F. Liu, S.-F. Yin, Bismuth complexes with N/S coordination based metallopolymer as highly efficient photocatalyst for selective oxidation of styrene, Fuel 302 (2021), 121127, https://doi.org/10.1016/j.fuel.2021.121127.
[6] S. Tian, B. Wang, W. Gong, Z. He, Q. Xu, W. Chen, Q. Zhang, Y. Zhu, J. Yang, Q. Fu, C. Chen, Y. Bu, L. Gu, X. Sun, H. Zhao, D. Wang, Y. Li, Dual-atom Pt heterogeneous catalyst with excellent catalytic performances for the selective hydrogenation and epoxidation, Nat. Commun. 12 (2021) 3181, https://doi.org/10.1038/s41467-021-23517-x.
[7] J. He, P. Lyu, B. Jiang, S. Chang, H. Du, J. Zhu, H. Li, A novel amorphous alloy photocatalyst (NiB/In_2O_3) composite for sunlight-induced CO_2 hydrogenation to HCOOH, Appl. Catal. B: Environ. 298 (2021), 120603, https://doi.org/10.1016/j.apcatb.2021.120603.
[8] J. Hu, R. Zhao, H. Li, Z. Xu, H. Dai, H. Gao, H. Yu, Z. Wang, Y. Wang, Y. Liu, J. Han, R. Guo, Boosting visible light photocatalysis in an Au@TiO_2 yolk-in-shell nanohybrid, Appl. Catal. B: Environ. 303 (2022), 120869, https://doi.org/10.1016/j.apcatb.2021.120869.
[9] S.G. Lee, M.J. Kang, M. Park, K.-j Kim, H. Lee, H.S. Kim, Selective photocatalytic conversion of benzyl alcohol to benzaldehyde or deoxybenzoin over ion-exchanged CdS, Appl. Catal. B: Environ. 304 (2022), 120967, https://doi.org/10.1016/j.apcatb.2021.120967.
[10] J. Li, H. Huang, W. Xue, K. Sun, X. Song, C. Wu, L. Nie, Y. Li, C. Liu, Y. Pan, H.-L. Jiang, D. Mei, C. Zhong, Self-adaptive dual-metal-site pairs in metal-organic frameworks for selective CO_2 photoreduction to CH_4, Nat. Catal. 4 (2021) 719–729, https://doi.org/10.1038/s41929-021-00665-3.
[11] M.Y. Qi, M. Conte, M. Anpo, Z.R. Tang, Y.J. Xu, Cooperative coupling of oxidative organic synthesis and hydrogen production over semiconductor-based photocatalysts, Chem. Rev. 21 (2021) 13051–13085, https://doi.org/10.1021/acs.chemrev.1c00197.
[12] Y. Huang, Z. Liu, G. Gao, G. Xiao, A. Du, S. Bottle, S. Sarina, H. Zhu, Stable copper nanoparticle photocatalysts for selective epoxidation of alkenes with visible light, ACS Catal. 7 (2017) 4975–4985, https://doi.org/10.1021/acscatal.7b01180.
[13] F. Li, J. Tang, Q. Ke, Y. Guo, M.N. Ha, C. Wan, Z. Lei, J. Gu, Q. Ling, V.N. Nguyen, W. Zhan, Investigation into enhanced catalytic performance for epoxidation of styrene over $LaSrCo_xFe_{2-x}O_6$ double perovskites: the role of singlet oxygen species promoted by the photothermal effect, ACS Catal. 11 (2021) 11855–11866, https://doi.org/10.1021/acscatal.1c03164.
[14] Y. Guo, L. Zhengwang, W. Guangjian, Y. Huang, F. Kang, Highly selective epoxidation of styrene over mesoporous Au-Ti-SBA-15 via photocatalysis process: synthesis, characterization, and catalytic application, Appl. Surf. Sci. 258 (2011) 1082–1090, https://doi.org/10.1016/j.apsusc.2011.09.010.
[15] M. Li, Y. Su, T. Xu, S. Wang, J. Bai, Template-free and in-situ growth of LZ-276&Alkali-impregnated carbon nanofibers for efficient epoxidation of styrene, Mater. Lett. 303 (2021), 130546, https://doi.org/10.1016/j.matlet.2021.130546.
[16] Z.K. Xin, Y.J. Gao, Y. Gao, H.W. Song, J. Zhao, F. Fan, A.D. Xia, X.B. Li, C.H. Tung, L.Z. Wu, Rational design of dot-on-rod nanoheterostructure for photocatalytic CO_2 reduction: pivotal role of hole transfer and utilization, Adv. Mater. (2021), 2106662, https://doi.org/10.1002/adma.202106662.
[17] Q. Guo, F. Liang, X.-B. Li, Y.-J. Gao, M.-Y. Huang, Y. Wang, S.-G. Xia, X.-Y. Gao, Q.-C. Gan, Z.-S. Lin, C.-H. Tung, L.-Z. Wu, Efficient and selective CO_2 reduction integrated with organic synthesis by solar energy, Chem 5 (2019) 2605–2616, https://doi.org/10.1016/j.chempr.2019.06.019.
[18] Q. Shi, Z. Li, L. Chen, X. Zhang, W. Han, M. Xie, J. Yang, L. Jing, Synthesis of SPR Au/$BiVO_4$ quantum dot/rutile-TiO_2 nanorod array composites as efficient visible-light photocatalysts to convert CO_2 and mechanism insight, Appl. Catal. B: Environ. 244 (2019) 641–649, https://doi.org/10.1016/j.apcatb.2018.11.089.
[19] Y. Zhao, G.I.N. Waterhouse, G. Chen, X. Xiong, L.Z. Wu, C.H. Tung, T. Zhang, Two-dimensional-related catalytic materials for solar-driven conversion of CO_x into valuable chemical feedstocks, Chem. Soc. Rev. 48 (2019) 1972–2010, https://doi.org/10.1039/C8CS00607E.
[20] Y. Zhao, S. Zhang, R. Shi, G.I.N. Waterhouse, J. Tang, T. Zhang, Two-dimensional photocatalyst design: a critical review of recent experimental and computational advances, Mater. Today 34 (2020) 78–91, https://doi.org/10.1016/j.mattod.2019.10.022.
[21] D. Huang, Z. Li, G. Zeng, C. Zhou, W. Xue, X. Gong, X. Yan, S. Chen, W. Wang, M. Cheng, Megamerger in photocatalytic field: 2D g-C_3N_4 nanosheets serve as support of 0D nanomaterials for improving photocatalytic performance, Appl. Catal. B: Environ. 240 (2019) 153–173, https://doi.org/10.1016/j.apcatb.2018.08.071.
[22] F. Raziq, A. Hayat, M. Humayun, S.K. Baburao Mane, M.B. Faheem, A. Ali, Y. Zhao, S. Han, C. Cai, W. Li, D.-C. Qi, J. Yi, X. Yu, M.B.H. Breese, F. Hassan, F. Ali, A. Mavlonov, K. Dhanabalan, X. Xiang, X. Zu, S. Li, L. Qiao, Photocatalytic solar fuel production and environmental remediation through experimental and DFT based research on CdSe-QDs-coupled P-doped-g-C_3N_4 composites, Appl. Catal. B: Environ. 270 (2020), 118867, https://doi.org/10.1016/j.apcatb.2020.118867.
[23] S. Gong, X. Teng, Y. Niu, X. Liu, M. Xu, C. Xu, L. Ji, Z. Chen, Construction of S-scheme 0D/2D heterostructures for enhanced visible-light-driven CO_2 reduction, Appl. Catal. B: Environ. 298 (2021), 120521, https://doi.org/10.1016/j.apcatb.2021.120521.
[24] M.Y. Ye, Z.H. Zhao, Z.F. Hu, L.Q. Liu, H.M. Ji, Z.R. Shen, T.Y. Ma, 0D/2D heterojunctions of vanadate quantum dots/graphitic carbon nitride nanosheets for enhanced visible-light-driven photocatalysis, Angew. Chem. Int. Ed. Engl. 56 (2017) 8407–8411, https://doi.org/10.1002/anie.201611127.
[25] P. Ma, X. Zhang, C. Wang, Z. Wang, K. Wang, Y. Feng, J. Wang, Y. Zhai, J. Deng, L. Wang, K. Zheng, Band alignment of homojunction by anchoring CN quantum dots on g-C_3N_4 (0D/2D) enhance photocatalytic hydrogen peroxide evolution, Appl. Catal. B: Environ. 300 (2022), 120736, https://doi.org/10.1016/j.apcatb.2021.120736.
[26] J. Wang, P. Kumar, H. Zhao, M.G. Kibria, J.G. Hu, Polymeric carbon nitride-based photocatalysts for photoreforming of biomass derivatives, Green Chem. 23 (2021) 7435, https://doi.org/10.1039/d1gc02307a.
[27] S. Xu, P. Zhou, Z.H. Zhang, C.J. Yang, B.G. Zhang, K.J. Deng, S. Bottle, H.Y. Zhu, Selective oxidation of 5–Hydroxymethylfurfural to 2,5–Furandicarboxylic acid using O_2 and a photocatalyst of Co-thioporphyrazine bonded to g-C_3N_4, J. Am. Chem. Soc. 139 (2017) 14775–14782, https://doi.org/10.1021/jacs.7b08861.
[28] F. Yuan, Z.M. Sun, C.Q. Li, Y. Tan, X.W. Zhang, S.L. Zheng, Multi-component design and in-situ synthesis of visible-light-driven SnO_2/g-C_3N_4/diatomite composite for high-efficient photoreduction of Cr(VI) with the aid of citric acid, J. Hazard. Mater. 396 (2020), 122694, https://doi.org/10.1016/j.jhazmat.2020.122694.
[29] X. Chen, Q. Wang, J. Tian, Y.Y. Liu, Y.D. Wang, C. Yang, A study on the photocatalytic sterilization performance and mechanism of Fe-SnO_2/g-C_3N_4 heterojunction materials, N. J. Chem. 44 (2020) 9456–9465, https://doi.org/10.1039/d0nj01137a.
[30] C.C. Chu, W. Miao, Q.J. Li, D.D. Wang, Y. Liu, S. Mao, Highly efficient photocatalytic H_2O_2 production with cyano and SnO_2 co-modified g-C_3N_4, Chem. Eng. J. 428 (2022), 132531, https://doi.org/10.1016/j.cej.2021.132531.
[31] S.X. Yu, J.Y. Li, Y.H. Zhang, M. Li, F. Dong, T.R. Zhang, H.W. Huang, Local spatial charge separation and proton activation induced by surface hydroxylation promoting photocatalytic hydrogen evolution of polymeric carbon nitride, Nano Energy 50 (2018) 383–392, https://doi.org/10.1016/j.nanoen.2018.05.053.
[32] F. Raziq, Y. Qu, M. Humayun, A. Zada, H. Yu, L. Jing, Synthesis of SnO_2/B-P codoped g-C_3N_4 nanocomposites as efficient cocatalyst-free visible-light photocatalysts for CO_2 conversion and pollutant degradation, Appl. Catal. B: Environ. 201 (2017) 486–494, https://doi.org/10.1016/j.apcatb.2016.08.057.
[33] J.L. Yang, D.Q. Cai, X.G. Hao, L. Huang, Q. Lin, X.T. Zeng, S.X. Zhao, W. Lv, Rich heterointerfaces enabling rapid polysulfides conversion and regulated Li_2S deposition for high-performance lithium-sulfur batteries, ACS Nano (2021), https://doi.org/10.1021/acsnano.1c01250.
[34] Y. Zhao, G. Liu, H. Wang, Y. Gao, T. Yao, W. Shi, C. Li, Interface engineering with an AlO_x dielectric layer enabling an ultrastable Ta_3N_5 photoanode for photoelectrochemical water oxidation, J. Mater. Chem. A 9 (2021) 11285–11290, https://doi.org/10.1039/D1TA00206F.
[35] Z. Opre, T. Mallat, A. Baiker, Epoxidation of styrene with cobalt-hydroxyapatite and oxygen in dimethylformamide: a green technology? J. Catal. 245 (2007) 482–486, https://doi.org/10.1016/j.jcat.2006.11.018.
[36] R.T. Chen, F.T. Fan, T. Dittrich, C. Li, Imaging photogenerated charge carriers on surfaces and interfaces of photocatalysts with surface photovoltage microscopy, Chem. Soc. Rev. 47 (2018) 8238–8262, https://doi.org/10.1039/C8CS00320C.
[37] R.S. Haider, S. Wang, Y. Gao, A.S. Malik, N. Ta, H. Li, B. Zeng, M. Dupuis, F. Fan, C. Li, Boosting photocatalytic water oxidation by surface plasmon resonance of Ag_xAu_{1-x} alloy nanoparticles, Nano Energy 87 (2021), https://doi.org/10.1016/j.nanoen.2021.106189.
[38] X. Yang, H. Sun, G. Li, T. An, W. Choi, Fouling of TiO_2 induced by natural organic matters during photocatalytic water treatment: Mechanisms and regeneration strategy, Appl. Catal. B: Environ. 294 (2021), 120252, https://doi.org/10.1016/j.apcatb.2021.120252.
[39] M. Li, S. Yu, H. Huang, X. Li, Y. Feng, C. Wang, Y. Wang, T. Ma, L. Guo, Y. Zhang, Unprecedented eighteen-faceted BiOCl with a ternary facet junction boosting cascade charge flow and photo-redox, Angew. Chem. Int. Ed. Engl. 58 (2019) 9517–9521, https://doi.org/10.1002/anie.201904921.
[40] Y. Zhang, D. Wang, W. Liu, Y. Lou, Y. Zhang, Y. Dong, J. Xu, C. Pan, Y. Zhu, Create a strong internal electric-field on PDI photocatalysts for boosting phenols degradation via preferentially exposing π-conjugated planes up to 100%, Appl. Catal. B: Environ. 300 (2022), 120762 https://doi.org/10.1016/j.apcatb.2021.120762.
[41] D. Zhu, Q. Zhou, Nitrogen doped g-C_3N_4 with the extremely narrow band gap for excellent photocatalytic activities under visible light, Appl. Catal. B: Environ. 281 (2021), 119474, https://doi.org/10.1016/j.apcatb.2020.119474.
[42] J. Jing, J. Yang, W. Li, Z. Wu, Y. Zhu, Construction of interfacial electric field via dual-porphyrin heterostructure boosting photocatalytic hydrogen evolution, Adv. Mater. (2021), 2106807, https://doi.org/10.1002/adma.202106807.
[43] G. Zhang, M. Liu, T. Heil, S. Zafeiratos, A. Savateev, M. Antonietti, X. Wang, Electron deficient monomers that optimize nucleation and enhance the photocatalytic redox activity of carbon nitrides, Angew. Chem. Int. Ed. Engl. 58 (2019) 14950–14954, https://doi.org/10.1002/anie.201908322.
[44] L. Ma, H. Zhou, X. Kong, Z. Li, H. Duan, An electrocatalytic strategy for C–C bond cleavage in lignin model compounds and lignin under ambient conditions, ACS Sustain. Chem. Eng. 9 (2021) 1932–1940, https://doi.org/10.1021/acssuschemeng.0c08612.
[45] X. Cao, Z. Chen, R. Lin, W.-C. Cheong, S. Liu, J. Zhang, Q. Peng, C. Chen, T. Han, X. Tong, Y. Wang, R. Shen, W. Zhu, D. Wang, Y. Li, A photochromic composite with enhanced carrier separation for the photocatalytic activation of benzylic C–H bonds in toluene, Nat. Catal. 1 (2018) 704–710, https://doi.org/10.1038/s41929-018-0128-z.
[46] Z. Li, L. Luo, M. Li, W. Chen, Y. Liu, J. Yang, S.M. Xu, H. Zhou, L. Ma, M. Xu, X. Kong, H. Duan, Photoelectrocatalytic C-H halogenation over an oxygen vacancy-rich TiO_2 photoanode, Nat. Commun. 12 (2021) 6698, https://doi.org/10.1038/s41467-021-26997-z.

[47] X. Wu, X. Fan, S. Xie, J. Lin, J. Cheng, Q. Zhang, L. Chen, Y. Wang, Solar energy-driven lignin-first approach to full utilization of lignocellulosic biomass under mild conditions, Nat. Catal. 1 (2018) 772–780, https://doi.org/10.1038/s41929-018-0148-8.

[48] V.H. Nguyen, J.C.S. Wu, H. Bai, Temperature effect on the photo-epoxidation of propylene over V–Ti/MCM-41 photocatalyst, Catal. Commun. 33 (2013) 57–60, https://doi.org/10.1016/j.catcom.2012.12.024.

[49] H. Hao, F. Zhang, X. Dong, X. Lang, 2D sp2 carbon-conjugated triazine covalent organic framework photocatalysis for blue light-induced selective oxidation of sulfides with O_2, Appl. Catal. B: Environ. 299 (2021), 120691, https://doi.org/10.1016/j.apcatb.2021.120691.

[50] Y. Zhang, N. Hatami, N.S. Lange, E. Ronge, W. Schilling, C. Jooss, S. Das, A metal-free heterogeneous photocatalyst for the selective oxidative cleavage of C-C bonds in aryl olefins via harvesting direct solar energy, Green Chem. 22 (2020) 4516–4522, https://doi.org/10.1039/D0GC01187H.

[51] P. Chaudhary, Deepa, D.R. Meena, M.J. Aalam, G.D. Yadav, S. Singh, Cellulose sulfate: an efficient heterogeneous catalyst for the ring-opening of epoxides with alcohols and anilines, Synth. Commun. 51 (2021) 1834–1846, https://doi.org/10.1080/00397911.2021.1910304.

[52] A. Das, N. Anbu, H. Reinsch, A. Dhakshinamoorthy, S. Biswas, A thiophene-2-carboxamide-functionalized Zr(IV) organic framework as a prolific and recyclable heterogeneous catalyst for regioselective ring opening of epoxides, Inorg. Chem. 58 (2019) 16581–16591, https://doi.org/10.1021/acs.inorgchem.9b02608.